


Adsorptive removal of Cr(VI) from aqueous solution: kinetic, isotherm, thermodynamics, toxicity, scale-up design, and GA modeling

Abhishek Das^{1,3} · Munmun Banerjee^{1,2} · Nirjhar Bar¹ · Sudip Kumar Das¹ 

© Springer Nature Switzerland AG 2019

Abstract

Chromium (VI) is a well-known toxic, industrial, water pollutant which has various, adverse effects on environmental health. Utilization of agricultural waste in effluent water treatment would minimize the problem of water pollution. The present study deals with the use of three types of nut shells for Cr(VI) removal. Adsorbents are characterized, using point of zero charges (pH_{pzc}), FTIR, BET surface area analysis, and SEM. The variation of different operating parameters on metal removal was conducted. The best sorption kinetic model was pseudo-second order. The adsorption process is both physical and chemical, and this depends on temperature. The Cr(VI) adsorption is spontaneous and endothermic. According to isotherm studies, Langmuir isotherm model fits fairly well for all adsorbents. Regeneration studies suggest that the adsorbents have proper regeneration criteria and can be used for multiple times. Study on RBC count of *Gallus gallus domesticus* gives concrete evidence of deadly effects of Cr(VI). It also figures out that the effluent solution treated with bio-adsorbents is less harmful. The scale-up design procedure is reported here. This study proved that groundnut shell, walnut shell, and almond shell have immense potential and can be utilized even after regeneration as replacement of commercial adsorbents for industrial wastewater. GA-ANN modeling has been developed for the best possible wastewater treatment management.

Keywords Groundnut shell · Walnut shell · Almond shell · Pseudo-second order · Langmuir model · Genetic algorithm

List of symbols

A_H	Harkins–Jura isotherm constant	D_e	Absorbate's effective diffusion coefficient in the adsorbent phase (m^2/s)
A_T	Equilibrium binding constant of Temkin isotherm (L/g)	E	Adsorption free energy (KJ/mol)
a_e	Adsorption rate (initial) (mg/(g min))	ΔG^0	Gibbs free energy change (kJ/mol)
B	Heat of adsorption (J/mol)	ΔH^0	Enthalpy change (kJ/mol)
B_H	Harkins–Jura isotherm constant	K	Fractional power model constant (mg/g)
b	Constant of Langmuir model (L/mg)	k_1	Rate constant of Lagergren model (min^{-1})
b_e	Chemisorption activation energy (g/mg)	k_2	Rate constant of pseudo-second-order model (g/mg min)
b_T	Constant of Temkin isotherm	K_{ad}	Rate constant of Natarajan and Khalaf model (min^{-1})
C	External convective mass transfer (mg/g)	K_f	Constant of Freundlich model (mg/g)/(mg/L) ^{1/n}
C_a	Cr(VI) ion concentration at the adsorbent at equilibrium (mg/L)	k_i	Rate constant of intraparticle diffusion model (mg/(g min ^{0.5}))
C_0	Cr(VI) ion concentration (initial) (mg/L)	K_c^0	Thermodynamic equilibrium constant
C_e	Cr(VI) ion concentration at equilibrium (mg/L)	K_c'	Apparent equilibrium constant
C_t	Ion concentration of Cr(VI) at time t (mg/L)		

✉ Sudip Kumar Das, skdchemengg@caluniv.ac.in; drsudipkdas@gmail.com | ¹Chemical Engineering Department, University of Calcutta, 92, APC Road, Kolkata 700009, India. ²Polymer Science and Technology Department, University of Calcutta, 92, APC Road, Kolkata 700009, India. ³Department of Microbiology, University of Calcutta, Ballygunge, Kolkata 700019, India.



SN Applied Sciences (2019) 1:776 | <https://doi.org/10.1007/s42452-019-0813-9>

Received: 7 March 2019 / Accepted: 19 June 2019 / Published online: 24 June 2019

n	Factor of heterogeneity
q_e	Sorption capacity at equilibrium (mg/g)
q_{\max}	Adsorption capacity of Langmuir isotherm, mg/g
q_s	Theoretical isotherm saturation capacity (mg/g)
q_t	Sorption capacity at time t (mg/g)
R	Ideal gas constant (J/(mol K))
R^2	Correlation coefficient
R_a	Adsorbent particle radius (m)
R_L	Dimensionless factor
ΔS^0	Change of entropy (kJ/mol K)
T	Temperature (K)
t	Time (min)
V	Solution volume (L)
ν	Fractional power model constant (min^{-1})
W	Adsorbent mass (g)
X_m	Maximum adsorption capacity of adsorbent (mmol/g)

Greek letters

λ	Constant related to sorption energy (mol^2/kJ^2)
ε	Polanyi potential (kJ^2/mol^2)

1 Introduction

Industrial wastes which are produced from textile, painting, leather, tanning, paper, cement, steel, and others get discharged into water bodies. This is harmful without any prior treatment given to the natural water bodies [1]. Chromium (VI) is the most toxic water pollutant among these heavy metals; it has six oxidation states; among them, hexavalent and trivalent are the most stable state. The high toxicity of Cr(VI) is a major concern as Cr(III) is relatively insoluble in water. Chromium (VI) has toxic effects on both animals and humans and is also a well-known carcinogen [2]. Longtime exposure to Cr(VI) causes dermatitis, ulcerations, and allergic skin reactions in the human body [3, 4].

To reduce water pollution, various treatment processes are practiced. Apart from adsorption, the other processes are precipitation, membrane separation, ion exchange, electrochemical precipitation, reverse osmosis, nanofiltration, and others [5, 6]. These techniques have their advantages as well as drawbacks [7–9]. Sludge formation with its disposal is the main drawback of the precipitation process. High operating cost diminishes the use of ion exchange as a better alternative. Due to the higher operating cost of other methods, the adsorption process is extensively used as an efficient, simple, economic water treatment process [10, 11].

Variety of agricultural waste like coconut shell, rice husk, shells of wheat, sawdust, wheat straw, shells of rice, pistachio, walnut, peanut, and almond is used as low-cost bio-adsorbent [12–14]. The synthetic adsorbents are appealing with respect to their adsorption capacity but its high

investment and preparation cost, hence, not suitable for rural industrial application, particularly in the Third World countries like India. So the green adsorbents, i.e., agricultural waste like nut shells, different leaves widely available in the rural areas without any cost, are the most suitable for adsorptive removal. The green adsorbent means natural adsorbents without any physical and chemical treatment [15]. Hence, in the batch mode Cr(VI) removal from aqueous solution by the shells of the groundnut, walnut, and almond is used as low-cost green adsorbents for the experimental investigation. Applicability of different kinetic and isotherm models is tested [16, 17]. Desorption studies have been tested to check their reusability criteria. The toxicity difference of metal-containing solution before and after adsorption on red blood cells (RBCs) of *Gallus gallus domesticus* is also investigated. The scale-up design procedure is reported.

Researchers used different artificial neural network (ANN) and genetic algorithm (GA)–ANN hybrid modeling to solve engineering problems [18–20]. The advantage of GA–ANN modeling over the ANN is evident in the less computational time required and gives better predictability. Hence, in the present study [21], the model parameters are optimized by using GA and then Lavenberg–Marquardt algorithm is used for the final prediction.

2 Experimental methodology

Groundnut, walnut, and almond shells are obtained from the local market, washed, and then dried at 105 °C temperature for 24 h. After this, dried shells are ground and sieved to prepare a size of 250–350 μm .

Merck analytical grade chemicals are used. The metal-stock solution of 1000 ppm is prepared by adding 2.8286 gm $\text{K}_2\text{Cr}_2\text{O}_7$ in 1000 ml distilled water. By diluting it, the desired solution is prepared.

The equipment used is as follows:

1. WTW pH meter (Multi 340i/SET, Germany)
2. BET (Quantachrome, Novawin 1000, USA)
3. FTIR (IS5Nicolet ATR, Thermo Fischer Scientific, USA)
4. UV–visible spectrophotometer (DR-5000 spectrophotometer, Hach, USA)
5. SEM (ZEISS, EVO-Q400 ++, Germany)

2.1 Experimental

Detailed of the experiment is given in our earlier paper [22, 23]. The Cr(VI) ion is analyzed by UV–visible spectrophotometer using 1,5 diphenyl carbazide coloring reagent at

540 nm [15, 16]. The amount of Cr(VI) adsorbed, and the removal percentage was calculated as,

$$q_t = \frac{(C_0 - C_t)V}{W} \quad (1)$$

$$\text{Removal percentage of metal ion} = \frac{(C_0 - C_t)}{C_0} \times 100 \quad (2)$$

Experiments were repeated thrice with reproducibility and relative deviation within the range of $\pm 0.5\%$ and $\pm 2.5\%$, respectively.

3 Results and discussion

3.1 Adsorbent characterization

Table 1 shows the results of FTIR analysis. It indicates that there are various activities, functional groups in fresh and Cr(VI)-loaded adsorbents. The existence of a broad peak indicates that phenolic or alcoholic –OH group is present in the adsorbents. This group involves in Cr(VI) adsorption as the peak of groundnut shell moves from 3310 to 3302 cm^{-1} , the peak of almond shell shifts from 3324 to 3331 cm^{-1} , and peak of walnut shell shifts from 3326 to 3300 cm^{-1} after adsorption. The frequency around 3310 cm^{-1} shows the existence of phenolic or alcoholic –OH group and shifts from 3310 to 3302 cm^{-1} indicating the chromium binding with (–OH) groups. At pH 1 or 2, H^+ ion neutralizes the (–OH) groups on the surface bearing and forms $-\text{OH}_2^+$ site that enhances the HCrO_4^- ion to adsorb. The aliphatic C–H stretching group is involved in adsorption of Cr(VI) as the peak moves from 2923 to 2920 cm^{-1} for groundnut shell, the peak of almond shell shifts from 2921 to 2934 cm^{-1} while the peak of walnut

shell shifts from 2903 to 2899 cm^{-1} . The aldehyde C–H stretching is also responsible for Cr(VI) adsorption for groundnut shell as the peak shifts from 2851 to 2854 cm^{-1} . Aliphatic acid C=O stretching takes part in Cr(VI) adsorption for groundnut shell and almond shell as the peak shifts from 1713 to 1734 cm^{-1} and 1735 to 1717 cm^{-1} , respectively. Alkene groups (C=C stretching) also interfere in the adsorption process, because peaks are shifted from 1620 to 1652 cm^{-1} (groundnut shell), 1636 to 1650 cm^{-1} (almond shell), 1607 to 1598 cm^{-1} (walnut shell) after adsorption. Aromatic groups (C=C stretching) on walnut shell peak move from 1509 to 1501 cm^{-1} . Peaks at 1414, 1418, and 1371 cm^{-1} indicate the carboxylic acid groups (C–O stretching) in the groundnut shell, almond shell, and walnut shell, respectively, and it shifts 1363, 1421, and 1325 cm^{-1} after adsorption. Peaks at 1226, 1230 and 1240 cm^{-1} are for stretching of C–O that indicate ester groups which are present in adsorbents and shifted after Cr(VI) adsorption. The wavelength of 1023 cm^{-1} (groundnut) and 1019 cm^{-1} (almond) and 1028 cm^{-1} (walnut) is for deformation of glycosidic C–H with OH bending and ring vibration. It indicates that there is a β glycosidic bond between glucose and cellulose [15, 16]. The peaks at 897, 890, and 889 cm^{-1} in Cr(VI)-loaded groundnut, almond, and walnut shell are indicative of the presence of Cr=O or Cr–O vibration which is responsible for Cr(VI) adsorption in the adsorbent surface.

SEM (Scanning Electron Microscope) images of fresh and Cr(VI)-loaded adsorbents are represented in Figs. 1a, b, 2a, b, 3a, b groundnut, walnut, and almond shell, respectively. SEM images of fresh adsorbents showed that the surface is porous and irregular, whereas for Cr(VI)-loaded adsorbents the SEM images are less porous. Cr(VI) ion is having crystal radius of 0.52 Å and binds with the various active groups which, in turn, blocked the pores partially [15, 16].

Table 1 FTIR analysis of fresh and Cr(VI)-loaded adsorbents

Functional groups	Peanut shell	Cr(VI) loaded peanut shell	Almond shell	Cr(VI) loaded almond shell	Walnut shell	Cr(VI) loaded walnut shell
Surface –OH stretching vibrations	3310	3303	3324	3331	3326	3300
Aliphatic C–H stretching	2923	2920	2921	2934	2903	2899
Aldehyde C–H stretching	2851	2854	x	x	x	x
Aliphatic acid C=O stretching	1713	1734	1735	1717	x	x
Unsaturated group like alkene C=C stretching	1620	1652	1636	1650	1607	1598
Aromatic C=C stretching	x	x	x	x	1509	1501
Carboxylic acid C–O stretching	1414	1363	1418	1421	1371	1325
Esters C–O stretch	1226	1244	1230	1225	1240	1244
Glycosidic C–H deformation with ring vibration and OH bending	1023	1019	1019	1013	1028	1030

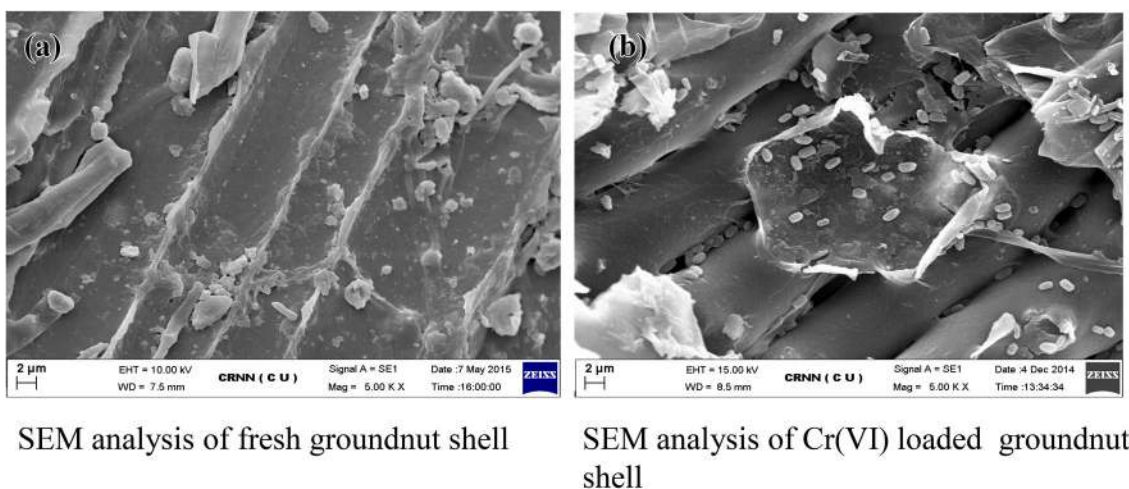


Fig. 1 **a** SEM analysis of fresh groundnut shell and **b** SEM analysis of Cr(VI)-loaded groundnut shell

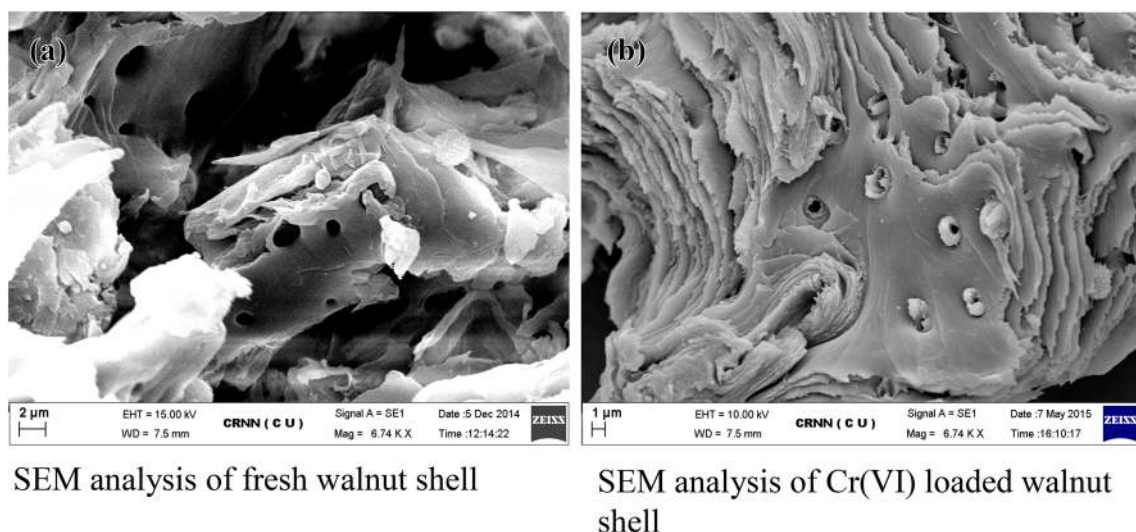


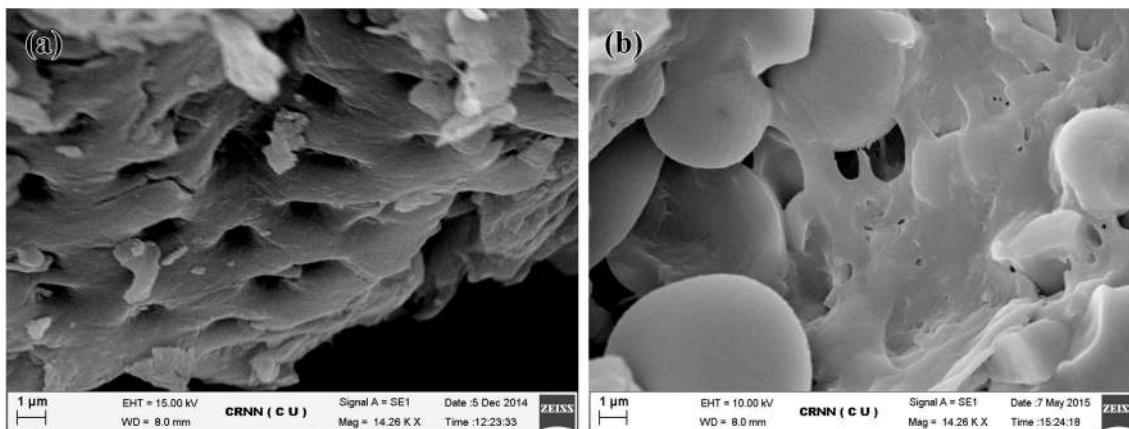
Fig. 2 **a** SEM analysis of fresh walnut shell and **b** SEM analysis of Cr(VI)-loaded walnut shell

The solid addition method is used to measure pH_{pzc} of the adsorbents [11, 24]. 30 mL of KNO_3 solutions (0.01 M) of different pH (3–10) was prepared. 0.1 g of bio-adsorbent was poured in each conical flask and equilibrated for the duration of 24 h. After that, the pH of supernatant solutions was measured. The intersection point between the initial pH and pH difference gives the value of pH_{pzc} . The similar procedure was carried out using 0.1 M KNO_3 solution. Adsorption of cations will be favorable at $\text{pH} > \text{pH}_{\text{pzc}}$ because, at this point, the surface of the adsorbents is negatively charged, which increases the electrostatic force of attraction. At lower pH ($\text{pH} < \text{pH}_{\text{pzc}}$), the positively charged adsorbent surface attracts anions. pH_{pzc} values are 6.21, 6.10, and 6.42 for groundnut, almond, and walnut shells, respectively.

The surface area of adsorbents is 1.83 m^2/gm , 11.27 m^2/gm , and 10.16 m^2/gm for groundnut, almond, and walnut shell, respectively, and determined using Brunauer–Emmett–Teller (BET) analysis.

3.2 Variation of operating parameters

The optimum pH of influent Cr(VI) solution is to achieve maximum removal efficiency by different nut shells. The maximum removal occurred at pH 2.0 for groundnut shell and walnut shell, whereas for the almond shell, it is found at pH 1.0 (Fig. 4). At low pH, the HCrO_4^- is predominant [10, 11]. At the acidic pH, large amount of H^+ ions is located onto the surface of the adsorbent and it creates a strong, attractive electrostatic force between the chromate ions



SEM analysis of fresh almond shell

SEM analysis of Cr(VI) loaded almond shell

Fig. 3 a SEM analysis of fresh almond shell and b SEM analysis of Cr(VI)-loaded almond shell

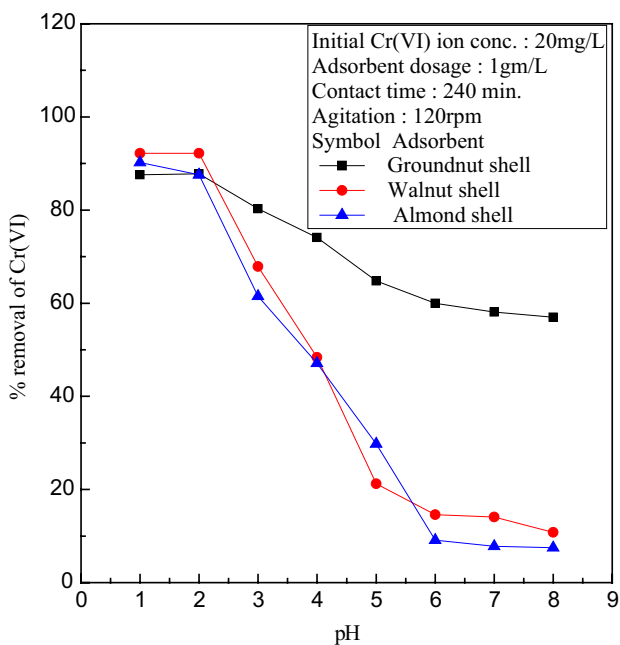


Fig. 4 Effect of pH on Cr(VI) adsorption

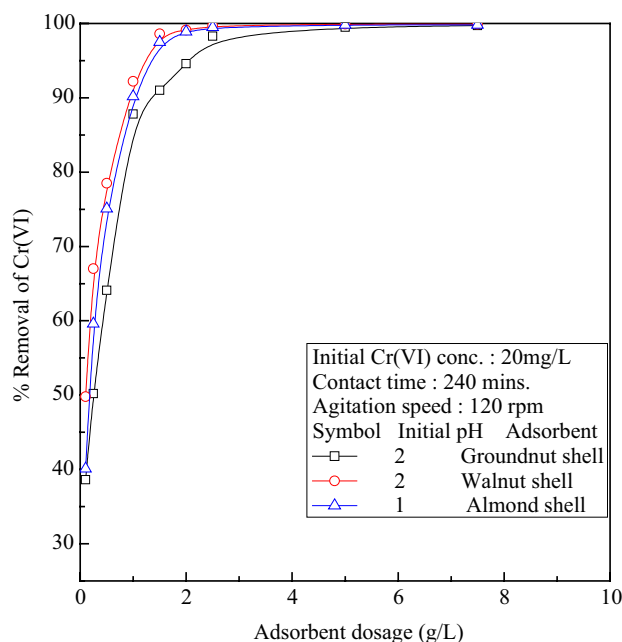


Fig. 5 Effect of adsorbate dosage on Cr(VI) adsorption

and adsorbent. As the $\text{pH} > 6.0$ the concentration OH^- ion increases and competes with CrO_4^{2-} ions to reach the active sites.

Effects of different adsorbent dosage were found by conducting experiments with varying amounts (0.1–8 gm/L). Figure 5 shows that the Cr(VI) removal increases with the increasing dosages of the adsorbent. It is also shown from the figure that the removal efficiency will remain the same after adsorbent dosages of 2.5 gm/L for groundnut shell and 1.5 gm/L for almond and walnut.

The metal binding sites for adsorption increase with the increase in adsorption dosage, but it remains constant for the higher dosages of the adsorbent.

Figure 6 shows the change of the Cr(VI) adsorption during different contact time. Agitation time for this study was set for 4–5 h. Initial adsorption was rapid and reached equilibrium at a prolonged rate. The nature of varying nut shells and their available adsorption sites affect the magnitude of equilibrium time. At the beginning, the adsorption rate was rapid, and more than 80% were absorbed within

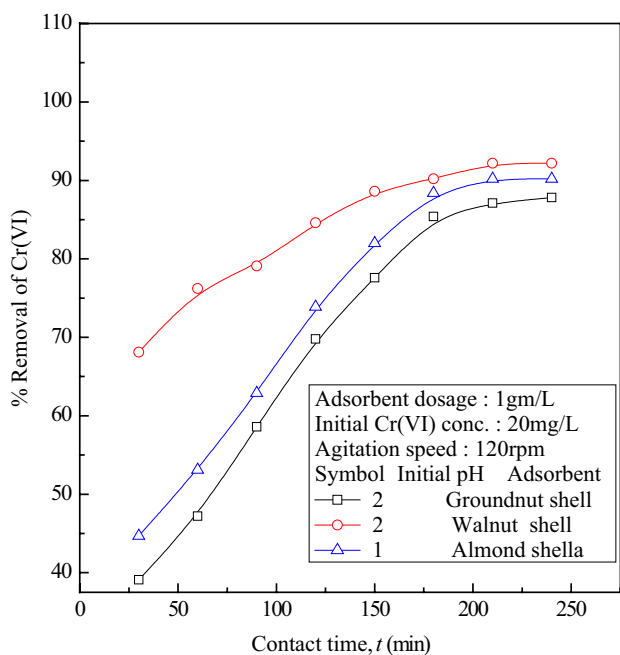


Fig. 6 Effect of contact time on Cr(VI) adsorption

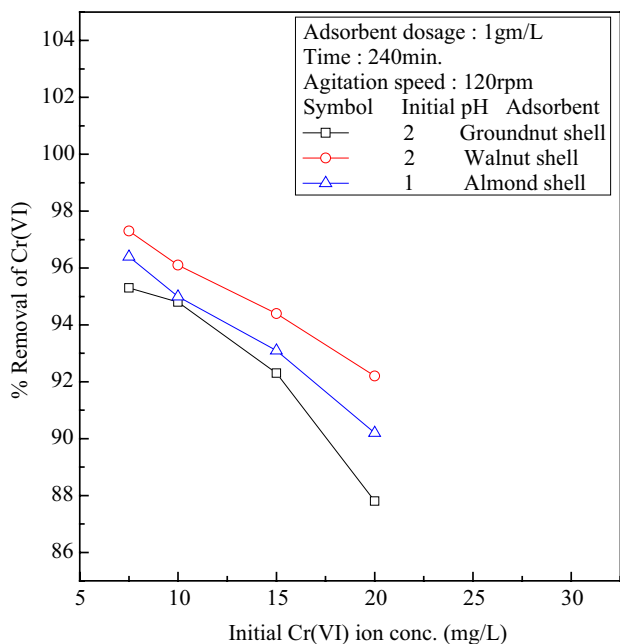


Fig. 7 Effect of initial Cr(VI) conc. on Cr(VI) adsorption

2 h for the walnut shell, and in the case for groundnut and almond shell, it took 4 h. After that, the rate of adsorption process decreases gradually and remains constant at equilibrium. Solution concentration will remain the same after reaching the equilibrium.

Figure 7 depicts the dependence of metal adsorption process with initial Cr(VI) concentrations (5–20 mg/L). The

figure indicates as the increase in the initial metal ion concentration, the percentage of removal decreases, whereas uptake capacity increases. At lower metal concentration, the numbers of available active sites on the adsorbent are much higher, but with the increase in initial metal ion concentration, the available active sites became saturated faster, hence decreasing the metal removal percentage.

3.3 Kinetics study

3.3.1 Pseudo-first-order model

Lagergren pseudo-first-order model is [25],

$$\ln(q_e - q_t) = \ln q_e - k_1 t \tag{3}$$

The parameters are estimated by plotting of $\ln(q_e - q_t)$ against t and listed in Table 2. The parameter k_1 has no specific trend with the increase in initial Cr(VI) concentration for groundnut and almond shell, whereas for walnut shell k_1 decreases as the Cr(VI) concentration increases. The R^2 values are not very impressive for all the adsorbents [26].

3.3.2 Pseudo-second-order model

This model [26] is:

$$\frac{t}{q_t} = \frac{1}{k_2 q_e^2} + \frac{t}{q_e} \tag{4}$$

The kinetic parameters are obtained from the plot of $\left(\frac{t}{q_t}\right)$ versus t and are shown in Table 2. The value of k_2 reduces with the increase in initial Cr(VI) concentration, and high R^2 value suggests that this model fits better for all adsorbents.

3.3.3 Elovich model

Second-order kinetics was described by the Elovich equation considering energetically heterogeneous solid surfaces [27]. But this model failed to explain the mechanism for adsorbate–adsorbent interaction. The linear model equation is as follows:

$$q_t = \frac{1}{b_e} \ln(a_e b_e) + \frac{1}{b_e} \ln t \tag{5}$$

By plotting q_t versus $\ln t$, the different model parameters were determined and are shown in Table 2. As the metal ion concentration increases, the magnitude of a_e increases, whereas the b_e decreases for groundnut shell. For walnut shell as the Cr(VI) concentration increases, both the parameter value reduced, and for the almond shell, no specific trend was observed. According to the value of R^2

Table 2 Different kinetic model parameters

Groundnut shell				
C_0 (mg/L)	7.5	10	15	20
Pseudo-first order				
k_1 (min^{-1}) $\times 10^{-2}$	1.9	2.6	2.8	2.5
q_{exp} (mg/g)	7.15	9.48	13.85	17.56
q_{cal} (mg/g)	9.43	24.17	47.8	39.8
R^2	0.89	0.80	0.71	0.92
Pseudo-second order				
k_2 (g/(mg min)) $\times 10^{-3}$	2.10	1.40	0.8	0.6
q_{exp} (mg/g)	7.15	9.48	13.85	17.56
q_{cal} (mg/g)	8.75	11.84	17.68	23.46
R^2	0.99	0.99	0.98	0.98
Elovich				
a_e (g/(gm min)) $\times 10^{-1}$	3.73	4.50	5.91	6.41
b_e (mg/g) $\times 10^{-1}$	5.36	3.97	2.65	1.91
R^2	0.97	0.97	0.95	0.96
Fractional power model				
K (mg/g)	1.13	1.18	1.75	1.74
ν (min^{-1})	0.34	0.39	0.38	0.43
R^2	0.98	0.99	0.97	0.97
Natarajan and Khalaf				
k_{ad} (min^{-1}) $\times 10^{-3}$	12.0	12.0	9.8	9.2
R^2	0.95	0.98	0.96	0.97
Intraparticle diffusion model				
k_i (mg/(g min ^{0.5})) $\times 10^{-1}$	3.8	5.2	7.9	10.8
C (mg/g)	1.59	1.77	2.10	1.74
R^2	0.98	0.99	0.98	0.97
Walnut shell				
Pseudo-first order				
k_1 (min^{-1}) $\times 10^{-2}$	3	3	2.8	2.4
q_{exp} (mg/g)	7.29	9.61	14.16	18.44
q_{cal} (mg/g)	4.39	8.32	13.93	16.17
R^2	0.87	0.95	0.93	0.94
Pseudo-second order				
k_2 (g/(mg min)) $\times 10^{-3}$	16.2	8.8	4.6	2.9
q_{exp} (mg/g)	7.29	9.61	14.16	18.44
q_{cal} (mg/g)	7.57	10.1	15.04	19.76
R^2	0.99	0.99	0.99	0.99
Elovich				
a_e (g/(mg min))	312.1	35.5	25.3	18.13
b_e (mg/g) $\times 10^{-1}$	15.6	9.04	5.64	3.99
R^2	0.98	0.98	0.97	0.98
Fractional power model				
K (mg/g)	4.42	4.95	7.24	8.1
ν (min^{-1})	0.01	0.13	0.13	0.15
R^2	0.95	0.95	0.98	0.98
Natarajan and Khalaf				
k_{ad} (min^{-1}) $\times 10^{-3}$	10.0	9.4	9.2	7.1
R^2	0.94	0.91	0.94	0.98

Table 2 (continued)

Walnut shell				
Intraparticle diffusion model				
k_i (mg/(g min ^{0.5})) × 10 ⁻¹	1.2	2.1	3.5	5.4
C (mg/g)	5.63	6.73	9.17	10.88
R^2	0.89	0.90	0.90	0.98
Almond shell				
Pseudo-first order				
k_1 (min ⁻¹) × 10 ⁻²	2.4	2.0	3.3	3.1
q_{exp} (mg/g)	7.23	9.5	13.97	18.04
q_{cal} (mg/g)	10.01	11.29	47.8	56.7
R^2	0.89	0.92	0.76	0.78
Pseudo-second order				
k_2 (g/(mg min)) × 10 ⁻³	3.4	2.2	1.1	0.7
q_{exp} (mg/g)	7.23	9.5	13.97	18.04
q_{cal} (mg/g)	8.3	11.11	17.25	22.94
R^2	0.99	0.99	0.98	0.98
Elovich				
a_e (g/(mg min)) × 10 ⁻¹	8.91	7.98	8.32	8.49
b_e (mg/g) × 10 ⁻¹	6.78	4.68	2.8	2.02
R^2	0.93	0.95	0.95	0.96
Fractional power model				
K (mg/g)	1.81	1.93	2.30	2.55
v (min ⁻¹)	0.27	0.29	0.34	0.37
R^2	0.96	0.95	0.95	0.98
Natarajan and Khalaf				
k_{ad} (min ⁻¹) × 10 ⁻³	14	11.3	12	9.2
R^2	0.96	0.96	0.95	0.95
Intraparticle diffusion model				
k_i (mg/(g min ^{0.5})) × 10 ⁻¹	3	4.3	7.3	11
C (mg/g)	2.89	3.17	3.35	2.58
R^2	0.95	0.97	0.96	0.98

and trend of parameters, application of Elovich model is significant for groundnut shell and walnut shell.

3.3.4 Fractional power model

Freundlich equation is modified to get the fractional power model [28] which can be described by the following linear equation:

$$\ln q_t = \ln K + v \ln t \tag{6}$$

Table 2 presents the value of both constants and other parameters. An increasing trend of K was noticed with the increase in initial Cr(VI) ion concentration for the ground nut-shell, but the value of v has no specific trend which limits its applicability for groundnut shell. For walnut and almond shell, both the constants decrease with the increase in initial Cr(VI) concentration. The v is a positive constant less

than unity and shows the time dependence of liquid-phase adsorption of Cr(VI) onto different nut shells. The value of K suggests the strength of the site for Cr(VI) binding. From Table 2, it can be observed that the strength of binding of Cr(VI) onto walnut shell is much stronger than the other nut shells used. The higher values of the correlation coefficient for all the three nutshells validate the appropriateness of fractional power.

3.3.5 Natarajan and Khalaf model

The kinetic equation of Natarajan and Khalaf model [29] is given as:

$$\log \left(\frac{C_0}{C_t} \right) = \left(\frac{k_{ad}}{2.303} \right) t \tag{7}$$

The value of k_{ad} is determined by plotting $\log\left(\frac{C_0}{C_t}\right)$ versus t and is shown in Table 2 and observed that as the initial metal concentration increases, the value of k_{ad} decreases for all three adsorbents.

The heterogeneous reversible first-order kinetics is the main assumption of this model. It explains the relationship between the concentration of initial and at time t . The high values of correlation coefficient signify that the adsorption process depends on the concentration of Cr(VI) at the aqueous solution at any given time. The high values of correlation coefficient signify that the adsorption process depends on the concentration of Cr(VI) at the aqueous solution at any given time. The correlation coefficient value R^2 for all adsorbents is less in comparison with pseudo-second-order model.

3.3.6 Intraparticle diffusion model

The adsorption process is a complex process with more than one rate-limiting step. Weber and Moris first explored the possibility of intraparticle diffusion-controlled adsorption process and developed a model equation for the same [30].

$$q_t = k_i t^{0.5} + C \quad (8)$$

Equation parameters are shown in Table 2. The intraparticle diffusional rate constant increases with the increase in initial Cr(VI) concentration. Though the R^2 value indicates the fitness of the equation, it has not passed through the origin; hence, it is not the rate-limiting step [30].

3.4 Rate-limiting step prediction

The adsorption mechanism has one or more than one rate-controlling mechanisms, just like chemical adsorption, film diffusion, or intraparticle diffusion of ions on the active sites of the surface. To illustrate Cr(VI) ion diffusion process on the pores of different bio-adsorbents, the equation of Fick's was used [10]

$$\frac{q_t}{q_a} = \frac{6}{R_a} \sqrt{\frac{D_e t}{\pi}} \quad (9)$$

q_a is replaced by q_e , and the plots of $\frac{q_t}{q_e}$ versus $t^{0.5}$ for groundnut shell, walnut shell, and almond shell depicted multi-linear segments and are presented in Fig. 8a–c. These figures indicated that more than one phenomenon governs the adsorption process. Even at the initial point of time, one factor may be rate controlling, which may change with time [31]. The plot of $\frac{q_t}{q_e}$ versus $t^{0.5}$ divided into three linear segments each of them represents the different mechanism of mass transfer. First linear segment

represents film diffusion mass transfer, second one represents intraparticle diffusion, and the last linear segment represents adsorption–desorption equilibrium. For groundnut shell, film diffusion segment took 79 min, whereas intraparticle diffusion took 1 min. For the walnut shell, film diffusion segment took 70 min, whereas intraparticle diffusion took 4 min. For the almond shell, film diffusion segment took 71 min, whereas intraparticle diffusion took 3 min. These signify that film diffusion mass transfer controls the entire adsorption process; this may be due to the formation of the thin film.

3.5 Adsorption isotherm models

3.5.1 Langmuir isotherm

This model is based on the monolayer adsorption on the homogeneous surface having energetically equivalent sites [32], and the linearized form is

$$\frac{C_e}{q_e} = \frac{1}{bq_{max}} + \frac{C_e}{q_{max}} \quad (10)$$

R_L a dimensionless factor is expressed as [15]

$$R_L = \frac{1}{1 + bC_0} \quad (11)$$

R_L values indicate that either the process is irreversible ($R_L = 0$) or linear ($R_L = 1$), favorable ($0 < R_L < 1$) or unfavorable ($R_L > 1$). Table 3 shows that q_{max} decreases as temperature increases for all the adsorbents, whereas the value of b increases for all the adsorbents. The values of R_L indicate favorable adsorption for all applied conditions for all the adsorbents [33]. According to the value of R^2 and the trend of parameters, application of the Langmuir model is highly significant for all the adsorbents.

3.5.2 Freundlich isotherm

It applies for multilayer adsorption and interaction of adsorbed molecules on the heterogeneous surface. This model considers an exponential decrease in sorption energy on adsorbent sorption centers completion [34]. Expression of this model is as follows:

$$\log q_e = \log K_f + \frac{1}{n} \log C_e \quad (12)$$

Table 3 shows the parameter and both the value of K_f and n increase as the temperature increases for all adsorbents. The parameter n must lie between 1 and 10 for favorable adsorption, and Table 3 indicates favorable adsorption for all adsorbents.

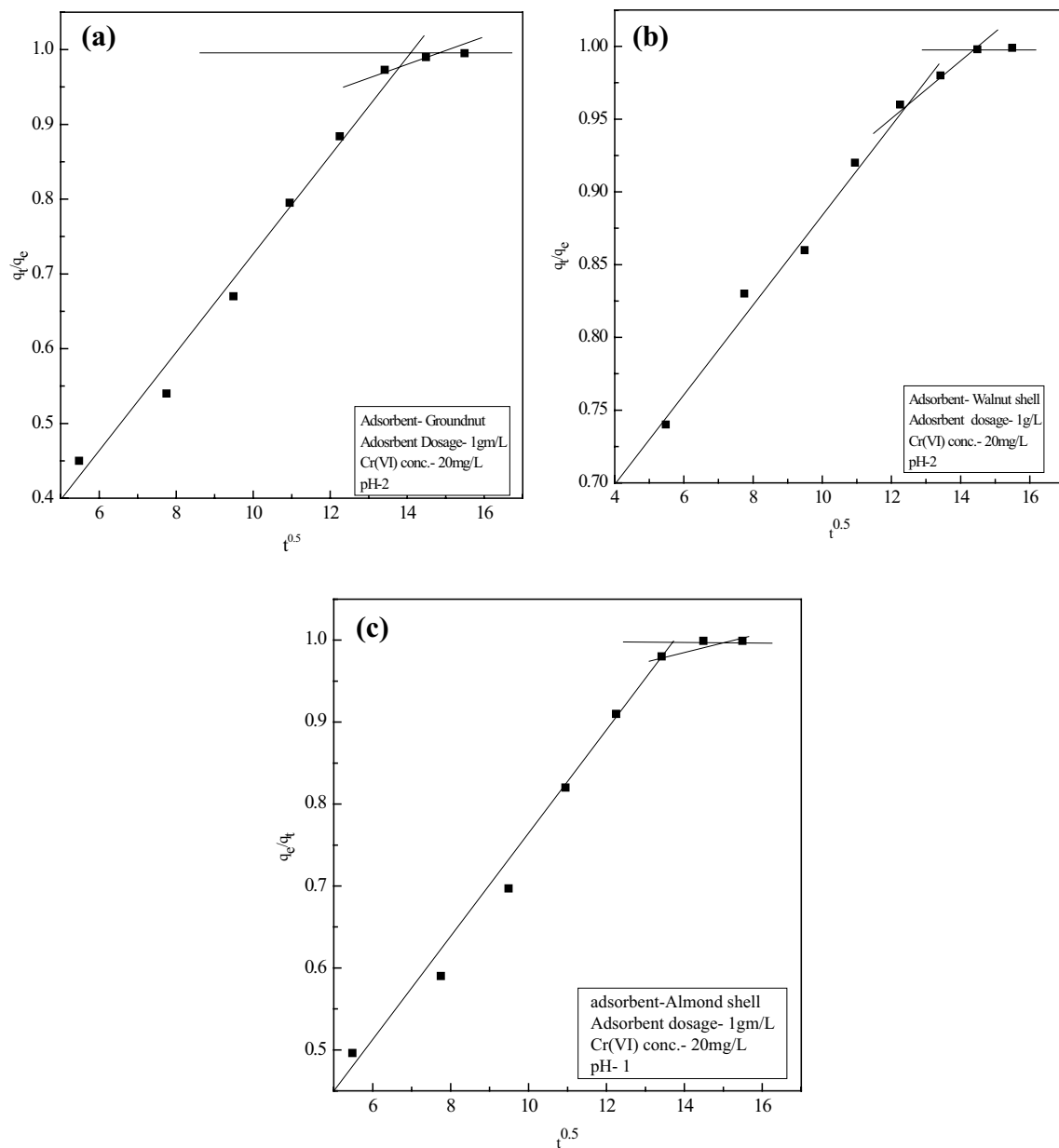


Fig. 8 **a** Plot of q_t/q_e versus $t^{0.5}$ for groundnut shell, **b** plot of q_t/q_e versus $t^{0.5}$ for walnut shell, and **c** plot of q_t/q_e versus $t^{0.5}$ for almond shell

3.5.3 Dubinin–Radushkevich isotherm

The isotherm equation [35, 36] is

$$\ln C_{\text{abs}} = \ln X_m - \lambda \epsilon^2 \tag{13}$$

Here ϵ is Dubinin–Radushkevich isotherm constant, and it has been also termed as Polanyi potential and is defined [37] by

$$\epsilon = RT \ln \left[1 + \frac{1}{C_e} \right] \tag{14}$$

The sorption energy E is estimated as

$$E = \frac{1}{\sqrt{-2\lambda}} \tag{15}$$

The value of E gives the nature of adsorption; for chemical adsorption, this value is $8 \text{ kJ/mol} < E < 16 \text{ kJ/mol}$, and for physical adsorption, it is $E < 8 \text{ kJ/mol}$. Table 3 indicates the physical adsorption for all adsorbents in the temperature 303 K and 313 K, but in the case of 323 K temperature, chemical adsorption occurs for all adsorbents.

Table 3 Different adsorption isotherm constants

Groundnut shell			
Temperature (K)	303	313	323
Langmuir model			
q_m (mg/g)	22.94	20.03	19.24
b (L/mg)	1.34	4.09	13.33
R_L ($C_0=7.5$ mg/L)	0.09	0.032	0.0099
R_L ($C_0=10$ mg/L)	0.069	0.024	0.007
R_L ($C_0=15$ mg/L)	0.05	0.02	0.005
R_L ($C_0=20$ mg/L)	0.04	0.012	0.004
R^2	0.99	0.99	0.99
Freundlich model			
K_f (mg/g)/(mg/L) ^{1/n}	12.13	15.1	16.65
n	2.38	3.18	5.74
R^2	0.98	0.98	0.95
Dubinin–Radushkevich model			
E (KJ/mol)	2.29	4.39	10.54
q_s (mg/g)	19.95	17.2	15.33
R^2	0.91	0.96	0.70
Temkin model			
A_T (L/g)	10.38	59.26	3053.4
b_T	454.2	690.5	1297.3
B (J/mol)	5.55	3.77	2.07
R^2	0.99	0.99	0.87
Harkins–Jura			
A_H	56.56	86.21	155.28
B_H	0.47	0.44	0.51
R^2	0.81	0.84	0.99
Walnut shell			
Temperature (K)	303	313	323
Langmuir model			
q_m (mg/g)	24.52	21.14	21.07
b (L/mg)	1.79	5.81	25
R_L ($C_0=7.5$ mg/L)	0.07	0.022	0.005
R_L ($C_0=10$ mg/L)	0.05	0.02	0.004
R_L ($C_0=15$ mg/L)	0.04	0.011	0.003
R_L ($C_0=20$ mg/L)	0.03	0.009	0.002
R^2	0.98	0.96	0.99
Freundlich model			
K_f (mg/g)/(mg/L) ^{1/n}	14.79	17.69	21.82
n	2.29	3.25	4.43
R^2	0.98	0.96	0.99
Dubinin–Radushkevich model			
E (KJ/mol)	2.94	5.98	9.57
q_s (mg/g)	20.78	16.61	17.81
R^2	0.83	0.78	0.86
Temkin model			
A_T (L/g)	12.68	114.89	1465.6
b_T	394.2	709.1	968.7
B (J/mol)	6.39	3.67	2.77

Table 3 (continued)

Walnut shell			
R^2	0.97	0.88	0.94
Harkins–Jura			
A_H	58.58	85.4	127.7
B_H	0.30	0.21	0.04
R^2	0.94	0.99	0.95
Almond shell			
Temperature (K)	303	313	323
Langmuir model			
q_m (mg/g)	24.25	20.12	19.78
b (L/mg)	1.40	4.70	17.54
R_L ($C_0 = 7.5$ mg/L)	0.087	0.03	0.008
R_L ($C_0 = 10$ mg/L)	0.07	0.02	0.006
R_L ($C_0 = 15$ mg/L)	0.05	0.014	0.004
R_L ($C_0 = 20$ mg/L)	0.034	0.011	0.003
R^2	0.99	0.99	0.99
Freundlich model			
K_f (mg/g)/(mg/L) ^{1/n}	12.83	15.37	18.17
n	2.38	3.42	5.21
R^2	0.99	0.99	0.94
Dubinin–Radushkevich model			
E (KJ/mol)	2.58	5.08	10.21
q_s (mg/g)	20.19	16.57	15.96
R^2	0.83	0.88	0.72
Temkin model			
A_T (L/g)	9.88	90.9	2186.4
b_T	397.97	743.51	1167.6
B (J/mol)	6.33	3.5	2.3
R^2	0.98	0.98	0.89
Harkins–Jura			
A_H	54.17	90.17	145.56
B_H	0.38	0.41	0.32
R^2	0.91	0.92	0.97

3.5.4 Temkin isotherm

This isotherm [38] was based on the interaction of adsorbent–adsorbate and refers that with the increase in surface coverage, the heat of adsorption increases.

$$q_e = \frac{RT}{b_T} \ln A_T + \frac{RT}{b_T} \ln C_e \tag{16}$$

The constant B (J/mol) can be calculated from

$$B = \frac{RT}{b_T} \tag{17}$$

Linear plot for Temkin adsorption isotherm gives values of A_T , b_T and B and is presented in Table 3. A_T and b_T values increase with the increase in temperature for all adsorbents, whereas the value of B decreases for the increase in temperature for all the adsorbents.

3.5.5 Harkins and Jura isotherm

This model that is originally applied for the gas–solid system is extended to solution–solid systems and assumed that condensed-type adsorbed films are formed on the adsorbent surface [39]. The isotherm is expressed as

$$\left(\frac{1}{q_e}\right)^2 = \left(\frac{B_H}{A_H}\right) - \left(\frac{1}{A_H}\right) \log C_e \tag{18}$$

As per Table 3, the value of A_H has an increase for all the adsorbent with the increase in temperature, whereas B_H decreases for the walnut shell. But no specific trends were found for the other two adsorbents. According to the correlation coefficient data, this model is not suitable for the Cr(VI) adsorption onto the nut shells.

From the statistical point of view, the Langmuir isotherm was the best-fitted isotherm for all the adsorbents used.

3.6 Thermodynamic studies

Three different temperatures (30, 40 and 50 °C) were chosen to describe the influence of temperature on Cr(VI) adsorption. The results show that the adsorption capacity of all three adsorbents is increased with the increase in temperature; hence, the adsorption process is facilitated by a higher temperature. The thermodynamic behavior [40] of the sorption was calculated from the following equations

$$\Delta G^0 = -RT \ln K_c^0 \quad (19)$$

and

$$\ln K_c^0 = \frac{\Delta S^0}{R} - \frac{\Delta H^0}{RT} \quad (20)$$

where the value of the thermodynamic equilibrium constant can be obtained from the apparent equilibrium constant, K_c' at different temperature and initial concentration of Cr(VI) for each adsorbent system and extrapolating to zero [10] where

$$K_c' = \frac{C_a}{C_e} \quad (21)$$

Table 4 shows the thermodynamic parameters as calculated. The negative value of ΔG^0 for all adsorbents indicates the spontaneous nature of Cr(VI) adsorption. Further, it decreases with the increase in temperature and shows that the degree of spontaneity increases at a higher temperature. The ΔG^0 value showed ranges between 0 and -20 kJ/mol which indicates the physisorption process [41].

Table 4 Thermodynamic parameters

Parameters	Temperature (K)	Groundnut shell	Walnut shell	Almond shell
ΔG^0 (kJ/mol)	303	-0.74	-1.47	-0.85
	313	-3.67	-4.58	-4.03
	323	-6.96	-8.64	-7.69
ΔS^0 (kJ/mol K)		317.5	366.6	349.7
ΔH^0 (kJ/mol)		95.49	109.75	105.2

Positive values of ΔS^0 reflect a increase in the degree of disorderliness at the adsorption interface during the adsorption of Cr(VI). The endothermic nature of the adsorption process by various nutshells was confirmed by the positive values of ΔH^0 [10, 42].

3.7 Mechanism of adsorption

The nature of nut shell's surface, different functional sites and their interaction behavior with adsorbing molecule govern the mechanism of adsorption. The FTIR spectra of fresh nut shells and Cr(VI) adsorbed nut shells suggest the possible interaction of Cr(VI) ion with phenolic or alcoholic -OH group. The spectral differences between the beginning of adsorption and after the adsorption suggest that the aliphatic C-H stretching and the aliphatic acid C=O stretching might take part in the adsorption process. The adsorbent pH_{pzc} value is important as it detects the ionic state of the adsorbent.

In this study, maximum adsorption occurs at lower pH 1 or 2 for the nut shells and is less than the pH_{pzc} . Hence, the active sites of the all the nut shells are charged positive [10, 11]. At low pH, chromium present in $HCrO_4^-$ form binds with the positively charged active groups by electrostatic attraction forces. The strength of electrostatic and hydrogen bonding interaction has been further confirmed from the result of Temkin and D-R isotherm models. D-R isotherm also indicates the governing of physical adsorption process in the temperature 303 K and 313 K, while at the 323 K temperature it shifts toward a chemical adsorption process for all the adsorbents. The weak interaction between Cr(VI) and the adsorbents can further be confirmed from the regeneration studies of different nut shells by changing the pH of the solution. The film diffusion is the main mass transfer process for Cr(VI) remotion in the nut shells.

3.8 Regeneration studies

Regeneration capability decides the usefulness of an adsorbent because multiple uses of adsorbent reduce the operational cost. NaOH solutions of different concentrations (0.1–0.75 M) used for desorption of Cr(VI) are presented in Table 5. This table indicates that as the concentration of NaOH solution increases, desorption of Cr(VI) also increases, which suggest that Cr(VI) adsorption is chemical [40]. Regeneration of the adsorbents was done up to second cycle, and Cr(VI) removal capacity after each desorption cycle is shown in Table 6 which depicts that with the successful regeneration of the adsorbents, the adsorption capacity decreases.

Table 5 Desorption of Cr(VI) from loaded adsorbents using different regenerant

Strength of NaOH (M)	Desorption percentage of Cr(VI) from loaded adsorbents		
	Groundnut Shell	Walnut Shell	Almond Shell
0.1	11	21	13
0.2	28	39	34
0.3	37	45	44
0.4	47	53	56
0.5	55	64	62
0.6	57	70	63
0.75	57	71	63

Table 6 Regeneration of adsorbents

Adsorbent	Cr(VI) removal percentage (%)		
	Fresh	After first regeneration	After second regeneration
Groundnut shell	87.8	69.8	41.5
Walnut shell	92.2	82.7	58.7
Almond shell	90.2	75.1	50.4

3.9 Comparison of the adsorptive capacities

The experimental adsorption capacity was compared with the other previously reported natural adsorbents and presented in Table 7. Adsorptive capacities of all these shells are quite good and comparable with others.

3.10 Effects on biological indicator (RBC)

3.10.1 Blood collection and separation of red blood cell (RBC)

Chicken blood sample was collected from Govt. recognized slaughter house (Chitpur Slaughter House, 400, Borough-II, B.K Paul Avenue, Rabindra Sarani, Garanhatta, Beniatola, Kolkata-700005, West Bengal, India). To prevent coagulation of collected blood sample from adult chicken (*Gallus gallus domesticus*), 2% EDTA solution was used [63]. Caution was taken while collecting the blood samples. Before the separation of RBC, the blood samples were cleaned by adding 0.9% saline solution in a centrifuge for 10 min at 1000 rpm. This procedure was repeated until the collection of fresh RBC.

Table 7 Comparison of Cr(VI) adsorption capacities of natural adsorbents

Serial no.	Adsorbent	Adsorption capacities q_{max} mg/g	References
1	Rice straw	12.17	[10]
2	Rice bran	12.34	[10]
3	Rice husk	11.39	[10]
4	Hyacinth root	15.28	[10]
5	Neem leaves	15.95	[10]
6	Coconut shell	18.69	[10]
7	Sugar beet Pulp	17.2	[43]
8	Maize cob	13.8	[43]
9	<i>Chlorella vulgaris</i>	23.0	[44]
10	<i>Scenedesmus obliquus</i>	15.6	[44]
11	Wheat straw black carbon	21.34	[45]
12	Hazelnut shell	17.70	[46]
13	Waste tyres	48.07	[47]
14	Coconut tree saw dust	3.46	[48]
15	Spent grain	18.94	[49]
16	Larch bark	15.8	[50]
17	Wool	41.15	[51]
18	Olive cake	33.44	[51]
19	Sawdust	15.82	[51]
20	Pine needles	21.50	[51]
21	Maple sawdust	0.14	[52]
22	<i>Fagus orientalis</i> L	16.13	[53]
23	<i>Agave lechuguilla</i>	6.6	[54]
24	Eucalyptus bark	45.00	[55]
25	Acorn of <i>Quercus ithaburensis</i>	31.48	[56]
26	Rice straw	3.15	[57]
27	Coconut coir	6.3	[58]
28	Jackfruit leaf	32.29	[59]
29	Mango leaf	35.7	[59]
30	Onion peel	19.88	[59]
31	Macadamia nutshell powder	45.23	[60]
32	Canadian peat	4.61	[61]
33	Coconut fiber	4.71	[61]
34	Raw coconut fiber	18.60	[62]
35	Groundnut shell	22.94	Present study
36	Walnut shell	24.52	Present study
37	Almond shell	24.25	Present study

3.10.2 Study of RBC

Three milliliters of RBC suspension was exposed to 500 µL of synthetic Cr(VI) solution of 20 mg/L concentration. In other batches, 3 ml of RBC suspension was exposed to 500 µL of different adsorbent-treated Cr(VI)

solutions, which is collected from the adsorption process at time intervals of 20, 60, and 120 min. After this, RBC suspensions were incubated for 1 h at 37 °C for further analysis. After the incubation period, RBC suspensions were washed three times. Then, slides are viewed and counted in the optical microscope (93309, Olympus microscope, Hemocytometer, India). The microscopic count at a different time interval of treatment is shown in Fig. 9.

3.10.3 Toxicity

In Fig. 9, untreated Cr(VI) solution showed decreasing RBC count after 1-h exposure as compared to the control. This result indicates that untreated Cr(VI) solution gives enough stress to the RBC. Application of treated Cr(VI) solution shows improvement in red blood cells count. As the increase in treatment time Cr(VI) percentage in solution decreases, which in turn recover the deficiency in RBC count.

4 Scale-up design

The mass balance equation for the adsorption process is [17]

$$V(C_0 - C_t) = Wq_t \tag{22}$$

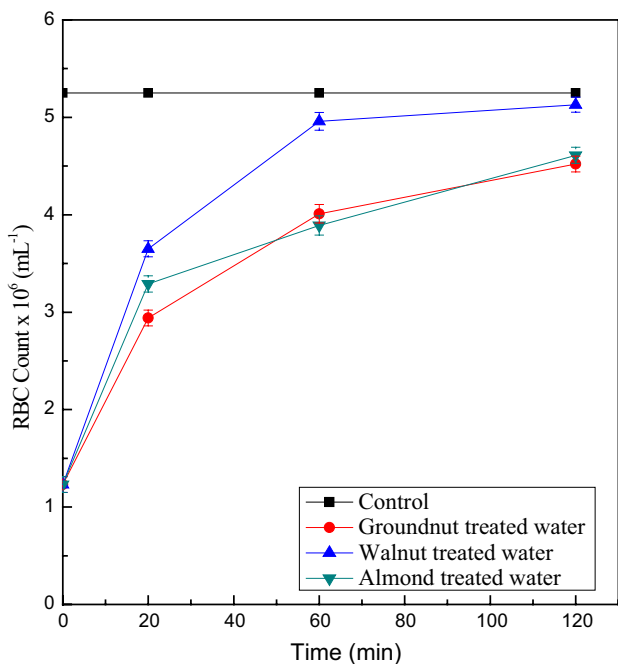


Fig. 9 Effects of untreated and treated Cr(VI) containing solution on RBC

When the system reaches equilibrium, the equation became

$$V(C_0 - C_e) = Wq_e \tag{23}$$

The best-fitted isotherm model for all the three systems is the Langmuir isotherm model, and this was used for design purpose. By combining the Langmuir isotherm equation with the mass balance equation, the following is obtained

$$\frac{W}{V} = \left(\frac{(C_0 - C_e)(bC_e + 1)}{bC_e q_{max}} \right) \tag{24}$$

From the sets of known values of b and q_{max} for the individual bio-adsorbents, the equation was further simplified, and a relationship for $\frac{W}{V}$ was obtained by using C_0 and C_e . Figure 10 shows the mass of walnut shell required to remove Cr(VI) ion at the initial concentration of 20 mg/L. Table 8 shows the adsorbent amount required for 80% remotion of Cr(VI).

5 Modeling of the network

Genetic algorithm (GA) is one of the techniques of optimization used in some cases during the last decade [20]. The use of a neural network to prune the choice of inputs is well documented in the past [63]. The use of the

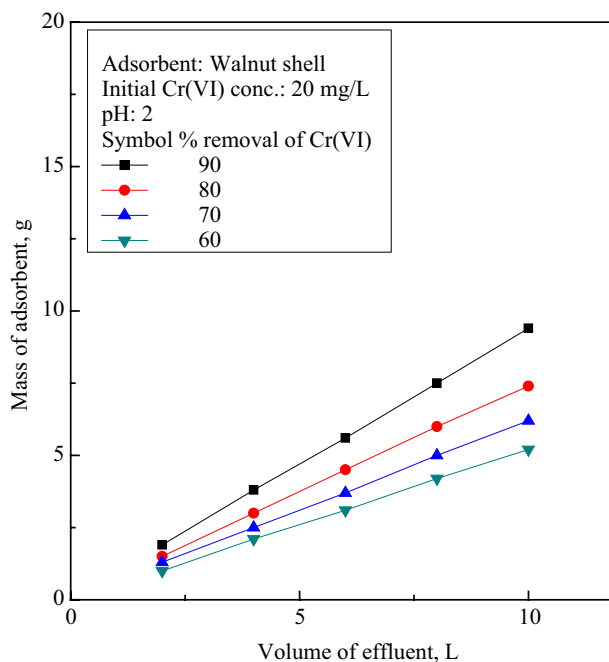


Fig. 10 Variation of minimum value of cross-validation with respect to number of processing elements in hidden layer

Table 8 Mass of adsorbent required for 80% Cr(VI) ions removal

Volume of effluent (L)	Groundnut shell (g)	Walnut shell (g)	Almond shell (g)
2	1.7	1.5	1.6
4	3.3	3.0	3.1
6	5.0	4.5	4.7
8	6.6	6.0	6.2
10	8.3	7.4	7.8

Levenberg–Marquardt algorithm (with the maximum of 1000 iterations and the possible application of stopping criterion within 100 iterations for improvement) for this purpose (optimize the number of nodes in the hidden layer within the value of 1–25) is also well documented. The choices of data that are not normalized are now a usual practice and are demonstrated in the past in our previous efforts [20, 21]. Therefore, this analysis is performed with the use of original data. The inputs of the GA are presented in Table 8 along with their range. Apart from the adsorbent number, the measurable quantities, e.g., pH, adsorbent dosage, contact time, temperature, and initial metal ion concentration, are considered. The predictable parameter, i.e., the output, is the percentage removal. For the elimination of the random error, the data have been independently randomized three times and are subsequently analyzed three times [63], and the predicted data are recorded. The division of data related to training, cross-validation, and the predicted output is divided into the usual 70, 20, and 10 percent, respectively, for the present study.

The roulette selection rule, the 1 point crossing overrule (crossover probability of 0.9), and the uniform mutation rule (mutation probability of 0.1) have been used. For the present analysis, the size of the population is chosen as 15 and 100 generations have been set for the evolution of the present GA network.

5.1 Network performance

Figure 11 shows the change in the MSE (minimum value of cross-validation) to that of the various generations for the three different randomizations. The optimized network can be considered keeping in mind the smallest numerical value achieved relating to the minimum value MSE for cross-validation during one of the generation numbers. Table 9 presents this MSE numerical value.

Table 10 represents the final performance of output regarding the statistical error parameters. The excellence of the performance is determined from the numeric value of the error parameters presented in Table 10. The observation yields the numerical value of

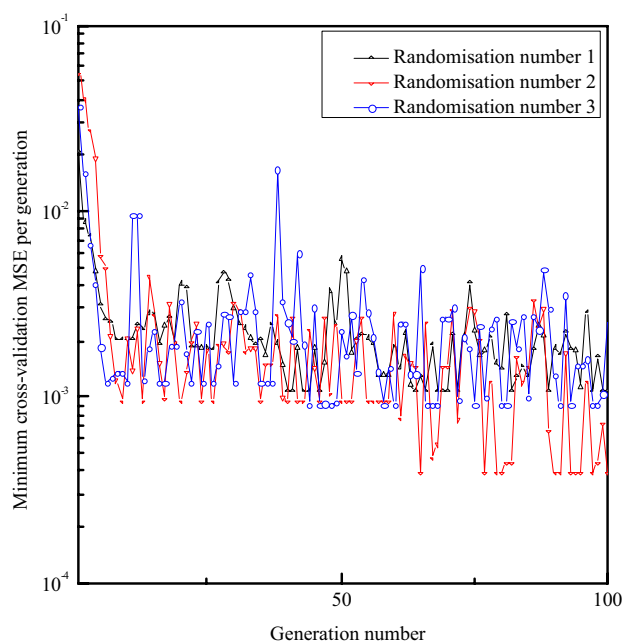


Fig. 11 Design of single batch adsorption system using Langmuir isotherm model for groundnut shells mass against volume of Cr(VI) ion containing aqueous solution at the initial concentration of 20 mg/L

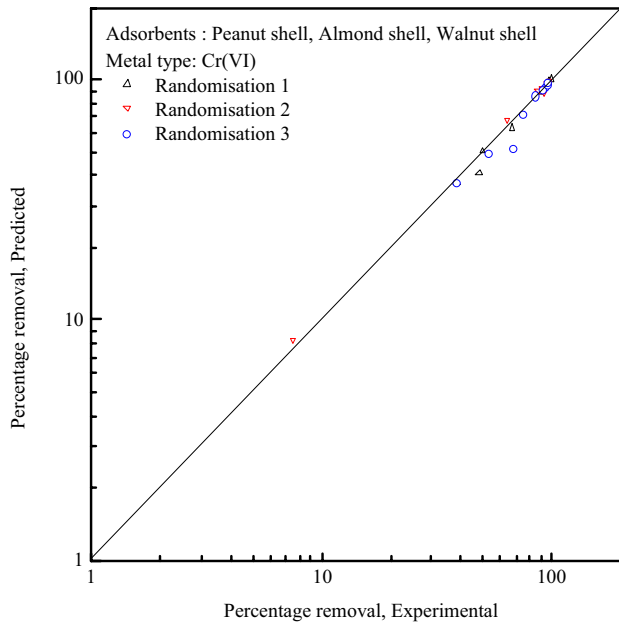
the cross-correlation coefficient (*R*) to be exceeding the lower limit of 0.97 to the upper limit 0.997. This alone presents the effectiveness of the modeling. This observation can also be ratified by the numerical value of the AARE and SD. The visual inspection of Fig. 12 indicates that the closeness of the output to the experimental data reiterates the excellent performance of the GA modeling (Table 10).

Table 9 Range of experimental and GA analysis data

Measurement type	Range
Input parameters	
Adsorbent number	1–3
pH	1–8
Adsorbent dosage (g/l)	0.1–2
Temperature (°C)	30–50
Contact time [<i>t</i> (min)]	15–240
Initial concentration [<i>C</i> ₀ (mg/l)]	7.5–20.0
Output parameter	
Percentage removal (%)	7.5–99.99
Total number of data points	93
Name of adsorbents	Peanut shell, almond shell, walnut shell

Table 10 Performance of the optimized hybrid network for three different randomizations for the prediction of percentage removal

Randomisation no.	Minimum MSE of cross-validation	AARE	SD (σ)	MSE	CCC (R)	χ^2
1	0.001079	0.036425	0.047484	9.376595	0.996147	1.786908
2	0.000385	0.031176	0.038012	5.135990	0.997108	0.662516
3	0.000907	0.043044	0.073009	29.04295	0.975954	5.028228

**Fig. 12** Comparison of percentage removal for experimental to the prediction

6 Conclusions

In this present study, groundnut shell, walnut shell, and almond shells were utilized to remove Cr(VI) in batch mode. The results of this investigation indicate that Cr(VI) adsorption depends on solution pH. Optimum pH for groundnut and walnut shell is 2, and for the almond, the shell is 1. The Cr(VI) removal efficiency of natural bio-adsorbents is quite high and is strongly dependent on operational parameters. The adsorption capacities of the nut shells are found to be 22.94 mg/g, 24.52 mg/g, and 24.25 mg/g, for the groundnut, walnut, and almond shells, respectively. Among the applied kinetic models, the pseudo-second order fits well for all three adsorbents. The prediction of rate-limiting steps reveals that film diffusion controls the Cr(VI) adsorption process for all three adsorbents. The Langmuir isotherm describes better process equilibrium than others. Dubinin–Radushkevich model predicts that Cr(VI) adsorption on groundnut shell, walnut shell, and almond shell are governed by both physical and chemical adsorption depending

on temperature. The adsorption process has also been found to be spontaneous and endothermic. The regeneration of the bio-adsorbents also finds its reusability as an adsorbent. Study of effects on RBC also gives a supporting proof of toxicity of Cr(VI) and the applicability of the used adsorbents for Cr(VI) removal. The scale-up design is also described. GA–ANN modeling successfully predicts metal removal. Lastly, easy availability with high adsorption capacity and good recovery make all of these three green bio-adsorbents a potential alternatives for the removal of toxic Cr(VI) ion from wastewater.

Compliance with ethical statements

Conflict of interest The authors declare that they have no conflict of interest.

References

- O'Connell DW, Birkinshaw C, O'Dwyer TF (2008) Heavy metal adsorbents prepared from the modification of cellulose: a review. *Biores Technol* 99:6709–6724
- Govind P, Madhuri S (2014) Heavy metals causing toxicity in animals and fishes. *Res J Anim Vet Fish Sci* 2(2):17–23
- Koren HS (1995) Associations between criteria air pollutants and asthma. *Environ Health Perspect* 103(Suppl 6):235–242
- Hu Q, Xiao Z, Xiong X, Zhou G, Guan X (2015) Predicting heavy metals' adsorption edges and adsorption isotherms on MnO₂ with the parameters determined from Langmuir kinetics. *J Environ Sci (China)* 27:207–216
- Ozer A, Altundogan HS, Erdem M, Tumen F (1997) A study on the Cr(VI) removal from aqueous solutions by steel wool. *Environ Poll* 97:107–112
- Namasivayam C, Yamuna RT (1995) Adsorption of chromium (VI) by a low-cost adsorbent: biogas residual slurry. *Chemosphere* 30:561–578
- Padilla AP, Tavani EL (1999) Treatment of an industrial effluent by reverse osmosis. *Desalination* 126:219–226
- Rengaraj S, Joo CK, Kim Y, Yi J (2003) Kinetics of removal of chromium from water and electronic process wastewater by ion exchange resins: 1200H, 1500H and IRN97H. *J Hazard Mater* 102:257–275
- Ahmed MT, Taha S, Chaabane T, Akretche D, Maachi R, Dorange G (2006) Nanofiltration process applied to the tannery solutions. *Desalination* 200:419–420
- Singha B, Das SK (2011) Biosorption of Cr(VI) ions from aqueous solutions: kinetics, equilibrium, thermodynamics and desorption studies. *Colloids Surf B Biointerfaces* 84:221–232

11. Banerjee M, Bar N, Basu RK, Das SK (2017) Comparative study of adsorptive removal of Cr(VI) ion from aqueous solution in fixed bed column by peanut shell and almond shell using empirical models and ANN. *Environ Sci Pollut Res* 24:10604–10620
12. Dupont L, Guillon E (2003) Removal of hexavalent chromium with a lignocellulosic substrate extracted from wheat bran. *Environ Sci Technol* 37:4235–4241
13. Singha B, Das SK (2013) Adsorptive removal of Cu (II) from aqueous solution and industrial effluent using natural/agricultural wastes. *Colloids Surf B Biointerfaces* 107:97–106
14. Siddiqui Sharf I, Chaudhry Saif A (2018) Nigella sativa plant based nanocomposite-MnFe₂O₄/BC: an antibacterial material for water purification. *Environ Res* 200:996–1008
15. Banerjee M, Bar N, Basu RK, Das SK (2018) Removal of Cr(VI) from its aqueous solution using green adsorbent pistachio shell: a fixed bed column study and GA-ANN modeling. *Water Conserv Sci Eng* 3(1):19–31
16. Banerjee M, Basu RK, Das SK (2018) Cr(VI) adsorption by a green adsorbent walnut shell: adsorption studies, regeneration studies, scale-up design and economic feasibility. *Proc Safe Environ Prot* 116:693–702
17. Banerjee M, Basu RK, Das SK (2019) Cu(II) removal using green adsorbents: kinetic modeling and plant scale-up design. *Environ Sci Pollut Res* 26(12):11542–11557
18. Bar N, Biswas MN, Das SK (2010) Prediction of pressure drop using artificial neural network for gas non-Newtonian liquid flow through piping components. *Ind Eng Chem Res* 49(19):9423–9429
19. Singha B, Bar N, Das SK (2014) The use of artificial neural networks (ANN) for modeling of adsorption of Cr(VI) ions. *Des Water Treat* 52(1–3):415–525
20. Ghaedi M, Daneshfar A, Ahmadi A, Momeni MS (2015) Artificial neural network-genetic algorithm based optimization for the adsorption of phenol red (PR) onto gold and titanium dioxide nanoparticles loaded on activated carbon. *J Ind Eng Chem* 21:587–598
21. Bahrami S, Ardejani FD, Baafi E (2016) Application of artificial neural network coupled with genetic algorithm and simulated annealing to solve groundwater inflow problem to an advancing openpit mine. *J Hydrol* 536:471–484
22. Naiya TK, Bhattacharya AK, Das SK (2008) Adsorption of Pb(II) by sawdust and neem bark from aqueous solutions. *Environ Prog* 27(3):313–328
23. Ilyas M, Ahmed A, Saeed M (2013) Removal of Cr(VI) from aqueous solutions using peanut shell as adsorbent. *J Chem Soc Pak* 35(3):760–768
24. Srivastava VC, Swamy MM, Mall ID, Prasad B, Mishra IM (2006) Adsorptive removal of phenol by bagasse fly ash and activated carbon: equilibrium, kinetics and thermodynamics. *Colloids Surf A Physicochem Eng Asp* 272:89–104
25. Lagergren S (1898) Zur theorie der sogenannten adsorption gelöster stoffe, *Kungliga Svenska Vetenskapakademiens. Handlingar* 24(4):1–39
26. Siddiqui Sharf I, Chaudhry Saif A (2019) Nanohybrid composite Fe₂O₃-ZrO₂/BC for inhibiting the growth of bacteria and adsorptive removal of arsenic and dyes from water. *J Clean Prod* 223:849–868
27. Rudzinski W, Panczyk T (2002) The Langmuirian adsorption kinetics revised: a farewell to the XXth century theories? *Adsorption* 8:23–34
28. Venkatesh R, Amudha T, Sivaraj R, Chandramohan M, Jambulingam M (2010) Kinetics and equilibrium studies of adsorption of direct Red-28 onto *Punica granatum* Carbon. *Int J Eng Sci Technol* 2(6):2040–2050
29. Shahul Hameed K, Sivakumar S, Satheesh Kannan R (2016) Isotherm and kinetic studies on the adsorption of Commassie Brilliant Blue on commercial activated carbon and kaolin. *Global J Adv Res* 3:723–731
30. Weber WJ, Morris JC (1963) Kinetics of adsorption on carbon from solution. *J Sanitary Eng Div* 89:31–60
31. Ho YS (2003) Removal of copper ions from aqueous solution by tree fern. *Water Res* 37:2323–2330
32. Langmuir I (1918) The adsorption of gases on plane surfaces of glass, mica and platinum. *J Am Chem Soc* 40(1918):1361–1403
33. Singha B, Das SK (2011) Biosorption of Cr(VI) ions from aqueous solutions: kinetics, equilibrium, thermodynamics and desorption studies. *Colloids Surf B Biointerfaces* 84(1):221–232
34. Freundlich HMF (1906) Über die adsorption in losungen. *Z Phys Chem* 57(A):385–470
35. Dubinin MM (1960) The potential theory of adsorption of gases and vapors for adsorbents with energetically non-uniform surface. *Chem Rev* 60:235–266
36. Dubinin MM, Zaverina ED, Radushkevich LV (1947) Sorption and structure of active carbons I. Adsorption of organic vapors. *Zh Fiz Khim* 21:1351–1362
37. Polanyi M (1932) Section III—theories of the adsorption of gases. A general survey and some additional remarks. *Trans Faraday Soc* 28:316–333
38. Temppin MI, Pyzhev V (1940) Kinetics of ammonia synthesis on promoted iron catalyst. *Acta Phys Chim USSR* 12:327–356
39. Harkins WD, Jura G (1943) An absolute method for the determination of the area of a fine crystalline powder. *J Chem Phys* 11:430
40. Bhattacharya AK, Naiya TK, Mandal SN, Das SK (2008) Adsorption kinetics and equilibrium studies on removal of Cr(VI) from aqueous solutions using different low-cost adsorbents. *Chem Eng J* 137(3):529–541
41. Siddiqui Sharf I, Chaudhry Saif A (2018) A review on graphene oxide and its composites preparation and their use for the removal of As³⁺ and As⁵⁺ from water under the effect of various parameters: application of isotherm, kinetic and thermodynamics. *Process Saf Environ Protect* 119:138–163
42. Siddiqui Sharf I, Chaudhry Saif A (2019) Nigella sativa seed based nanocomposite-MnO₂/BC: an antibacterial material for photocatalytic degradation, and adsorptive removal of dye from water. *Environ Res* 171:328–340
43. Sharma DC, Foster CF (1994) A preliminary examination into the adsorption of hexavalent chromium using low-cost adsorbents. *Bioresour Technol* 47:257–264
44. Donmez GC, Aksu Z, Ozturk A, Kutsal T (1999) A comparative study on heavy metal biosorption characteristics of some algae. *Process Biochem* 34:885–892
45. Wang XS, Chen LF, Li FY, Chen KL, Wan WY, Tang YJ (2010) Removal of Cr(VI) with wheat-residue derived black carbon: reaction mechanism and adsorption performance. *J Hazard Mater* 175:816–822
46. Cimino G, Passerini A, Toscano G (2000) Removal of toxic cations and Cr(VI) from aqueous solution by hazelnut shell. *Water Res* 34:2955–2962
47. Hamadi NK, Chen XD, Farid MM, Lu MGQ (2001) Adsorption kinetics for the removal of chromium (VI) from aqueous solution by adsorbents derived from used tyres and sawdust. *Chem Eng J* 84:95–105
48. Selvi K, Pattabhi S, Kadirvelu K (2001) Removal of Cr(VI) from aqueous solution by adsorption onto activated carbon. *Bioreour Technol* 80:87–89
49. Low KS, Lee CK, Low CH (2001) Sorption of chromium (VI) by spent grain under batch conditions. *J Appl Polym Sci* 82:2128–2134
50. Aoyama M, Tsuda M (2001) Removal of Cr(VI) from aqueous solutions by larch bark. *Wood Sci Technol* 35(5):425–434

51. Dakiky M, Khamis M, Manassra A, Mer'eb M (2002) Selective adsorption of chromium(VI) in industrial wastewater using low-cost abundantly available adsorbents. *Adv Environ Res* 6:533–540
52. Yu LJ, Shukla SS, Dorris KL, Shukla A, Margrave JL (2003) Adsorption of chromium from aqueous solutions by maple sawdust. *J Hazard Mater B* 100:53–63
53. Acar FN, Malkoc E (2004) The removal of chromium(VI) from aqueous solutions by *Fagus orientalis* L. *Biores Technol* 94(1):13–15
54. Romero-González Peralta-Videoa JR, Rodríguez E, Ramirez SL, Gardea-Torresdey JL (2005) Determination of thermodynamic parameters of Cr(VI) adsorption from aqueous solution onto *Agave lechuguilla* biomass. *J Chem Thermodyn* 37:343–347
55. Sarin V, Pant KK (2006) Removal of chromium from industrial waste by using eucalyptus bark. *Biores Technol* 97:15–20
56. Malkoc E, Nuhoglu Y (2007) Determination of kinetic and equilibrium parameters of the batch adsorption of Cr(VI) onto waste acorn of *Quercusithaburensis*. *Chem Eng Process* 46:1020–1029
57. Gao H, Liu Y, Zeng G, Xu W, Li T, Xia W (2008) Characterization of Cr(VI) removal from aqueous solutions by a surplus agricultural waste rice straw. *J Hazard Mater* 150(2):446–452
58. Gonzalez MH, Georgia L, Claudia BP, Eveline M (2008) Coconut coir as biosorbent for Cr(VI) removal from laboratory wastewater. *J Hazard Mater* 159(2–3):252–256
59. Nag S, Mondal A, Bar N, Das SK (2017) Bio-sorption of chromium (VI) from aqueous solutions and ANN modeling. *Environ Sci Poll Res* 24:18817–18835
60. Pakade VE, Ntuli TD, Ofomaja AE (2017) Biosorption of hexavalent chromium from aqueous solutions by macadamia nutshell powder. *Appl Water Sci* 7:3015–3030
61. Chwastowski J, Staroń P, Kołoczek H, Banach M (2017) Adsorption of hexavalent chromium from aqueous solutions using Canadian peat and coconut fiber. *J Mol Liq* 248:981–989
62. Fernanda PF, Tannous K, Coppi CC (2019) Biosorption of hexavalent chromium from aqueous solutions using raw coconut fiber as a natural adsorbent. *Chem Eng Commun* 1:1. <https://doi.org/10.1080/00986445.2018.1557154>
63. Nag S, Mondal A, Nath Roy A, Bar N, Das SK (2018) Sustainable bioremediation of Cd(II) from aqueous solution using natural waste materials: kinetics, equilibrium, thermodynamics, toxicity studies and GA-ANN hybrid modeling. *Environ Technol Innov* 11:83–104

Publisher's Note Springer Nature remains neutral with regard to jurisdictional claims in published maps and institutional affiliations.